PHYSICAL REVIEW A **95**, 052702 (2017)

Electron-impact dissociation and ionization of CN^+ ions

D. S. Belic,[1,*] X. Urbain,[2] H. Cherkani-Hassani,[3] and P. Defrance[2]

[1]*Faculty of Physics University of Belgrade, P.O. Box 386, Belgrade 11000, Serbia*

[2]*Institute of Condensed Matter and Nanosciences, Université Catholique de Louvain, Louvain-la-Neuve 1348, Belgium*

[3]*Université Sidi Mohamed Ben Abdellah, Faculté des Sciences Dhar El Mahraz, B.P. 1796, Fès-Atlas 30003, Morocco*

(Received 3 March 2017; published 10 May 2017)

Absolute cross sections are reported for electron-impact ionization and dissociation of CN^+ ions. Simple ionization to CN^{2+} ions and formation of singly charged C^+ and N^+ and doubly charged C^{2+} and N^{2+} fragments have been investigated. The animated electron-ion crossed-beam method has been applied in the energy range from the respective reaction thresholds up to 2.5 keV. The maximum of the simple ionization cross section is found to be $(5.37 \pm 0.14) \times 10^{-18}$ cm^2 at 115 eV. The maximum total cross sections for N^+ and C^+ fragment production are found to be $(22.2 \pm 2.7) \times 10^{-17}$ and $(18.9 \pm 1.2) \times 10^{-17}$ cm^2 at 85 eV, respectively. By performing careful magnetic field scans of the collected ions, contributions of dissociative excitation and dissociative ionization to the C^+ and N^+ fragment production are determined separately. The cross sections for asymmetric dissociative ionization to C^{2+} and N^{2+} are found to be more than one order of magnitude smaller. The kinetic energy release distributions are determined for all dissociation processes at selected electron energies. These distributions, together with the energy thresholds, provide additional information about the ground and excited states of the molecular ion.

DOI: 10.1103/PhysRevA.95.052702

I. INTRODUCTION

CN is a fundamental molecule found in numerous environments, ranging from the sun's atmosphere to terrestrial plasmas and within flames [1]. It has been observed in a variety of different astronomical phenomena [2–5]. Its anion, CN^-, was one of the first molecular anions detected in the interstellar medium. The CN rotational spectrum has been used to measure the temperature of the cosmic microwave background along different lines of sight [6,7]. Within these diverse environments CN can undergo a variety of processes.

In this paper we concentrate on electron collisions with the CN radical cation or cyanogen ion, CN^+. Information on electron scattering is important as such collisions may cause electronic excitations, as well as ionization and dissociation to various fragments. This produces the electronic emission spectra crucial in identifying the molecule in a range of environments, but also emphasizes the role of such species regarding the radiative balance of terrestrial plasmas. At the same time these processes have an important impact on the energy and particle balance of various discharges and plasmas including thermonuclear fusion. Electron collisional excitation of CN was considered some time ago by Crawford *et al.* [8] and Allison and Dalgarno [9], and recently by Harrison and Tennyson [10] and Harrison *et al.* [11].

The cyanogen molecule radical, CN, has a $^2\Sigma^+$ symmetry in its ground electronic state. Its cation CN^+ has a $^1\Sigma^+$ symmetry with the $1\sigma^2 2\sigma^2 3\sigma^2 1\pi^4$ configuration and is isoelectronic with C_2. While the $^3\Pi$ state correlates to the $C^+(^2P) + N(^4S)$ limit, the $^1\Sigma^+$ state correlates to the $C(^3P) + N^+(^3P)$ limit. It does, however, dissociate to the $C^+(^2P) + N(^2D)$ limit due to an avoided crossing with the first excited $^1\Sigma^+$ state. This will influence the outcome of the dissociative excitation process, as discussed below.

Extended-basis self-consistent field configuration interaction (SCF-CI) potential curves for the low-lying $^3\Pi$, $^1\Sigma^+$, $^1\Pi$, and $^3\Sigma^+$ states of CN^+ are examined by Murrell *et al.* [12]. They found that the nature of the ground state, whether $^3\Pi$ or $^1\Sigma^+$, depends on the quality of the CI treatment undertaken. Their most extensive calculation makes these two states almost degenerate. Another extensive CI study was undertaken by Bruna [13] for the $^1\Sigma^+$ and $^3\Pi$ states of the CN^+ ion at their respective equilibrium geometries. All calculations in which the reference configurations contribute significantly to the final CI vectors (and similar amounts to both states) place the $^1\Sigma^+$ state lower than $^3\Pi$ by 0.10–0.20 eV.

Large-scale CI calculations are reported also by Bruna *et al.* [14] for the potential curves of a series of diatomic systems isovalent to CN^+, in their lowest electronic states. The CI method used is of the multireference double-excitation (MRD-CI) variety, including individualized configuration selection and energy extrapolation. By including up to 17 reference species to generate the MRD-CI spaces (of orders up to 150 000) and by supplementing the atomic orbitals (AO) basis with f functions it is found that the ground state of CN^+ is the $\pi^4\ ^1\Sigma^+$ species (as in isovalent C_2) falling 0.1 eV below the $\sigma\pi^3\ ^3\Pi$ state. This result is in significant disagreement with earlier theoretical predictions on this point, which have generally tended to place the $^3\Pi$ state at least 0.3 eV below the $^1\Sigma^+$ state.

More recently Hirst [15] performed a comprehensive theoretical treatment of the low-lying states of the molecular ion CN^+ correlating with $C^+(^2P) + N(^4S)$ and with $C^+(^2P) + N(^2D)$. The calculations employ good-quality basis sets and electron correlation is taken into account by extensive configuration interaction. Spectroscopic constants are derived from the potential-energy curves for the bound states, and the calculated values are useful predictions for states which have not yet been observed. Electric dipole moment functions and electronic transition moments have been calculated.

*belicd@ff.bg.ac.rs

Complete basis set and Gaussian *ab initio* computational study of dissociative recombination and dissociative excitation processes of the cyanogen ion was published by Jursic [16]. Ionization potentials and electron affinities for several atoms and diatomic molecules involved in the dissociative recombination and dissociation process of the cyanogen ion were calculated.

There is relatively little experimental information about the excited states of the CN^+ ion despite its astrophysical importance. An interesting study was carried out by Reid [17] about state composition of CN^+ beams formed from electron-impact-ionized HCN, C_2N_2, and NH_2CN, and term energies of observed long-lived states ($^3\Pi$ and $^3\Sigma^+$).

Electronic-state analyses of 6-keV beams of CN^+ ions have been carried out through translational-energy spectroscopy of products formed in Xe or CS_2 target gas. All beams were found to contain CN^+ ions in the $a\ ^3\Pi$ state, of term energy 0.12 ± 0.20 eV, while beams formed using electrons also contained CN^+ ions in a triplet state ($^3\Sigma^+$) of 1.32 ± 0.10 eV term energy. The proportions of $^1\Sigma^+$, $^3\Pi$, and $^3\Sigma^+$ ions in the beam formed from 100-eV electroionized HCN were estimated to be 0.80, 0.11, and 0.09, and the $^3\Pi$-to-$^1\Sigma^+$ population ratio was found to increase with decreasing electron energy, to about 30:70 at the CN^+ appearance threshold of 20 ± 1 eV. In the beam formed from C_2N_2 (or NH_2CN) the $^3\Pi$ and $^3\Sigma^+$ proportions were 0.35 and 0.16 at 100 eV. The remaining 49% was $^1\Sigma^+$, and no significant variation of the $^3\Pi$-to-$^1\Sigma^+$ population ratio with decreasing electron energy was detected. Under certain circumstances, electron capture by CN^+ ($^3\Pi$) ions was found to be less efficient than capture by CN^+ ($^1\Sigma^+$) ions and thus beam composition may be an important factor in reactivity studies involving this cation.

An extensive experimental study of electron impact on the cyanogen ion was performed by Le Padellec *et al.* [18]. Absolute cross sections of the dissociative recombination and excitation of the CN^+ ($X\ ^1\Sigma^+$ and $a\ ^3\Pi$, $v = 0$) were measured in a merged electron ion beam configuration, by using the heavy-ion storage ring CRYRING in Stockholm. Cross sections for the dissociative excitation process are also reported and their magnitude at the plateau is found to be unusually large.

Electron collisions with the species of interest for the astrophysical and plasma physics community, for low-energy discharges as well as for the fusion plasma, are currently investigated in our laboratory. The animated electron-ion crossed beam experiment is used, designed to measure electron-impact dissociation and ionization cross sections of molecular ions. A number of diatomic molecules and some radicals have been studied recently. For instance, electron-impact ionization and dissociation of CO^+ [19], CD^+ [20], NH^+, and ND^+ [21,22], and more recently of OH^+ and OD^+ ions [23] and NO^+ [24], were investigated in detail.

In the present work, the following reactions are investigated:

$$CN^+ + e^- \rightarrow CN^{2+} + 2e^- \quad (19.47\ \text{eV}), \tag{1}$$

$$\rightarrow C + N^+ + e^- \quad (8.28\ \text{eV}), \tag{2}$$

$$\rightarrow C^+ + N + e^- \quad (4.97,7.57\ \text{eV}), \tag{3}$$

$$\rightarrow C^+ + N^+ + 2e^- \quad (19.47\ \text{eV}), \tag{4}$$

$$\rightarrow C + N^{2+} + 2e^- \quad (37.75\ \text{eV}), \tag{5}$$

$$\rightarrow C^{2+} + N + 2e^- \quad (29.22,31.81\ \text{eV}). \tag{6}$$

Reaction (1) is simple ionization (SI), with the cross section denoted as σ_{SI}. Reactions (2) and (3) represent dissociative excitation (DE) processes for N^+ and C^+ fragment production, denoted as σ_{01} and σ_{10}, respectively. Subscripts refer to the charge states of the C and N fragments, respectively.

Reaction (4) is dissociative ionization (DI), a process in which single ionization is followed by dissociation of the intermediate dication to two singly charged (C^+ and N^+) fragments, and is denoted by σ_{11}. Obviously, detection of either C^+ or N^+ should produce an identical value of σ_{11}. Finally, reactions (5) and (6) represent asymmetric dissociative ionization (ADI) processes, leading to the formation of the doubly charged fragments N^{2+} and C^{2+}, respectively, with corresponding cross sections σ_{02} and σ_{20}. Threshold energies cited in parentheses are from Ref. [16]. Where indicated, the first and second thresholds correspond to N(^4S) and N(^2D) production, respectively.

The total absolute cross sections σ_{C^+} and σ_{N^+} for C^+ and N^+ products represent the sums of DE and DI cross sections for each fragment, respectively. In another words, $\sigma_{C^+} = \sigma_{10} + \sigma_{11}$ and $\sigma_{N^+} = \sigma_{01} + \sigma_{11}$.

Moreover, other processes are also possible, such as electron attachment followed by ion pair dissociation, referred to as resonant ion pair formation, or simply dissociative electron attachment, referred to as dissociative recombination (DR) [25]. This electron capture may be followed by the autoionization of the molecular system in its dissociation continuum, in which case it contributes to dissociative excitation and is referred to as resonant dissociative excitation (RDE) [26]. This is discussed, in connection with the σ_{C^+} and σ_{N^+} cross sections, later in the text.

The experimental setup, the procedure, and the data analysis method are described hereafter. Present results are compared with the existing data from the literature.

II. EXPERIMENTAL PROCEDURE

In the present experiment, the animated crossed electron-ion-beam technique is used [27]. It is described elsewhere in detail [19] and only a brief overview is given here. The molecular ion beam is produced in an electron-cyclotron-resonance (ECR) ion source by introduction of CO and N_2 simultaneously. The beam (12 keV) interacts at a right angle to the tunable energy electron beam, from a few up to 2.5 keV. Product ions are separated from the primary ion beam in a double-focusing 90° magnetic analyzer. They are further purified by a 90° electrostatic spherical deflector and directed onto the channel electron multiplier.

The animated electron-ion-beam method consists in sweeping the electron beam across the ion beam at a constant speed u. The total number of events, K, produced during one complete electron beam sweep is related to the measured cross section σ_m by

$$\sigma_m = \frac{uK}{I_e I_i \gamma} \frac{v_e v_i q_i e^2}{\left(v_e^2 + v_i^2\right)^{1/2}}, \tag{7}$$

where γ is the detector efficiency, I_e and I_i are the electron- and ion-beam current intensities, and e, $q_i e$, v_e, and v_i are the charges and velocities of electrons and ions, respectively. The detection efficiency of the channel electron multiplier (Sjuts KBL25RS) was measured by the beam sweeping method [28], yielding $\gamma = 0.95 \pm 0.05$ for D^+ at 6 keV. The possible evolution of this efficiency over the course of the measurement was monitored by regular measurements of a benchmark cross section, i.e., the single ionization of Ne^+ at 200 eV.

In the simple ionization process (1), the total signal is detected and the cross section is readily determined by Eq. (7). On the contrary, reactions (2)–(6) are dissociative two-step processes; the target is first excited to a repulsive intermediate state from which it immediately dissociates, thereby transferring internal energy to the kinetic energy of the fragments. As a result, dissociation products exhibit a broad velocity and angular distribution in the laboratory frame that exceeds the actual detector acceptance at a given magnetic field.

The apparent cross section $\sigma_m(B)$ is thus measured, at a given electron energy, as a function of the analyzer magnetic field B. Next, the velocity distribution is computed from this cross-section scan, and the total cross section σ is obtained by integrating this distribution over the whole velocity range [19]. The transmission efficiency of the experiment, defined as the ratio of the apparent cross section $\sigma_m(B)$ to the total cross section σ, is determined for several energies and extrapolated to the entire considered electron energy range. This efficiency is used to calculate total absolute cross sections.

Furthermore, the kinetic energy release (KER) distribution of the investigated fragment is derived [19] from the above velocity distribution. E_{KER} represents the total kinetic energy released to both dissociation fragments. The shape of the KER distribution depends on the various channels involved in the reaction, the number of which increases with electron energy. Below the ionization threshold, only DE is observed. Above that threshold, Coulomb repulsion is experienced by the DI fragments, resulting in significantly larger E_{KER}. In most cases, the two contributions, DE and DI, can be successfully separated on energy- and momentum-conservation grounds.

Analyzer magnetic field scans may thus be used (i) to estimate the absolute total cross sections, (ii) to separate DE and DI contributions and determine their absolute cross sections, and (iii) to determine the kinetic energy release distributions to the dissociation fragments.

The total uncertainty is estimated to be about 2% for SI, of the order of 10% for the total absolute cross sections, and, at a maximum, to be about 15% for the dissociative contributions (90% confidence limit). The uncertainty associated with the electron energy is estimated to be ±0.5 eV.

III. RESULTS AND DISCUSSION

In this section absolute cross sections, threshold energies, and kinetic energy release distributions are presented for electron-impact simple ionization of CN^+, for C^+ and N^+ fragment production (including both DE and DI contributions), and for asymmetric dissociative ionization processes leading to the C^{2+} and N^{2+} fragments, respectively. The results are obtained in the incident electron energy range from thresholds up to 2500 eV. Absolute cross sections for simple ionization (σ_{SI}) are listed in Table I. The total cross sections for dissociation to singly charged fragments, N^+ (σ_{N^+}) and C^+ (σ_{C^+}), are presented in Secs. III B and III C, respectively. These cross sections are listed in Tables II and III, and in both cases corresponding DE and DI contributions are also included. The cross sections for asymmetric dissociative ionization to C^{2+} and N^{2+} fragments are listed in Table IV. The results are presented in detail and discussed in the following paragraphs.

TABLE I. Absolute cross sections for electron-impact simple ionization of CN^+ (in 10^{-18} cm^2).

E (eV)	σ_{SI}	$\Delta\sigma_{\mathrm{SI}}$	E (eV)	σ_{SI}	$\Delta\sigma_{\mathrm{SI}}$
19.1	− 0.04	0.08	85.1	5.1	0.13
20.1	0.12	0.09	95.1	5.26	0.13
21.1	0.18	0.09	95.1	5.3	0.16
22.1	0.33	0.09	115.1	5.37	0.14
23.1	0.43	0.07	135.1	5.1	0.15
24.1	0.73	0.09	155.1	5.0	0.15
25.1	1.03	0.09	195.1	4.56	0.14
26.1	1.20	0.10	245.1	4.21	0.12
27.1	1.38	0.09	295.1	3.79	0.12
28.1	1.65	0.14	395.1	3.44	0.1
30.1	2.08	0.12	495.1	2.93	0.09
33.1	2.46	0.13	595.1	2.68	0.09
35.1	2.68	0.13	595.1	2.59	0.07
40.1	3.02	0.13	795.1	2.31	0.08
45.1	3.46	0.12	995.1	1.93	0.07
55.1	4.22	0.12	1495.1	1.5	0.06
65.1	4.80	0.13	1995.1	1.25	0.04
75.1	5.04	0.12	2495.1	1.0	0.04

A. Simple ionization, CN^{2+} production

Absolute cross sections for simple ionization, σ_{SI}, reaction (1), are determined directly from the measured quantities by using Eq. (7). The results are listed in Table I, together with the associated error bars, and also shown in Fig. 1. The maximum ionization cross section σ_{SI} is found to be $(5.37 \pm 0.14) \times 10^{-18}$ cm^2 at an electron energy of 115 eV. The threshold energy is determined, by linear extrapolation, to be 21.5 ± 0.5 eV. As in some previous experiments [21,24], a small contribution is found below this value, which appears down to 19.4 eV. This indicates that a fraction of ions of the primary ion beam may be vibrationally or even electronically excited [15,16]. This should be expected here, bearing in mind that the ions are not created by a direct ionization process, but by ion-molecule reactions in a N_2 and CO mixture. The value of threshold energy, however, is in fairly good agreement with the results determined by Kostko *et al.* [29] for the vertical transition energy in the Franck-Condon region. They have performed both vacuum-ultraviolet (VUV) photoionization experiments and close-coupling theoretical calculations. For the lower ionization potential values they listed energies of 20.46, 20.66, 20.8, and 22.2 eV. An extended multireference CI calculation of 13 quasibound CN^{2+} electronic states was published more recently by Fišer and Polák [30], who predict an adiabatic ionization energy of 25.5 eV. To the authors'

TABLE II. Total (σ_{N^+}), DE (σ_{01}), and DI (σ_{11}) cross sections (in 10^{-17} cm^2) for N^+ production by electron impact on CN^+.

E (eV)	σ_{N^+}	$\Delta\sigma_{N^+}$	σ_{01}	$\Delta\sigma_{01}$	$\sigma_{11}(N^+)$	$\Delta\sigma_{11}$
4.1	− 0.08	0.35	− 0.08	0.35		
5.1	0.69	0.33	0.69	0.33		
6.1	1.39	0.42	1.39	0.42		
7.1	2.22	0.344	2.22	0.34		
8.1	3.05	0.76	3.05	0.76		
9.1	3.89	0.78	3.89	0.78		
10.1	5.06	0.96	5.06	0.96		
12.1	6.90	1.05	6.90	1.05		
13.1	7.42	1.08	7.42	1.08		
15.1	8.49	1.17	8.49	1.17		
17.1	9.59	1.30	9.59	1.30		
19.1	11.47	1.59	11.36	1.59	0.11	0.42
21.1	12.62	1.68	12.27	1.68	0.16	0.46
25.1	13.82	1.82	12.82	1.82	1.00	0.56
30.1	15.95	2.05	13.60	2.05	2.35	0.70
35.1	17.70	2.14	14.06	2.14	3.64	0.86
40.1	18.92	2.32	14.38	2.32	4.54	0.91
45.1	19.05	2.38	13.43	2.38	5.62	1.04
55.1	20.21	2.46	12.98	2.46	7.23	1.18
65.1	21.67	2.67	13.24	2.67	8.43	1.04
75.1	21.45	2.60	12.10	2.60	9.35	1.21
85.1	22.24	2.74	12.31	2.74	9.94	1.23
95.1	21.94	2.78	11.79	2.78	10.15	1.23
115.1	22.03	2.63	11.55	2.63	10.48	1.26
135.1	21.15	2.61	10.63	2.61	10.52	1.27
155.1	20.21	2.35	9.72	2.35	10.49	1.33
195.1	18.44	2.07	8.41	2.07	10.03	1.34
245.1	16.53	2.05	7.01	2.05	9.53	1.19
295.1	14.81	2.05	6.21	2.05	8.60	1.09
395.1	12.97	1.81	5.14	1.81	7.83	1.07
495.1	11.77	1.63	5.03	1.63	6.34	0.81
595.1	10.23	1.42	4.40	1.42	5.83	0.81
795.1	8.68	1.27	3.71	1.27	4.97	0.73
995.1	7.143	1.11	3.26	1.11	3.89	0.62
1495.1	5.023	0.79	1.93	0.79	3.10	0.53
1995.1	3.94	0.68	1.71	0.68	2.23	0.43
2495.1	3.54	0.58	1.54	0.58	2.00	0.31

TABLE III. Total (σ_{C^+}), DE (σ_{10}), and DI (σ_{11}) cross sections (in 10^{-17} cm^2) for C^+ production by electron impact on CN^+.

E (eV)	σ_{C^+}	$\Delta\sigma_{C^+}$	σ_{10}	$\Delta\sigma_{10}$	$\sigma_{11}(C^+)$	$\Delta\sigma_{11}$
3.1	− 1.00	2.00	0.00	2.00		
4.1	2.12	2.00	2.12	2.00		
5.1	3.50	2.00	3.50	2.00		
6.1	8.43	1.66	8.43	1.66		
7.1	10.87	1.19	10.87	1.19		
8.1	10.83	1.40	10.83	1.40		
9.1	11.74	2.03	11.74	2.03		
10.1	11.03	1.60	11.03	1.60		
11.1	9.91	1.79	9.91	1.79		
12.1	10.01	1.66	10.01	1.66		
13.1	9.34	1.73	9.34	1.73		
15.1	10.16	1.32	10.16	1.32		
17.1	9.86	1.29	9.86	1.29		
19.1	11.12	1.18	11.00	1.18	0.11	0.42
21.1	11.26	1.33	10.99	1.33	0.26	0.46
25.1	11.19	0.77	10.09	0.77	1.10	0.56
30.1	12.34	1.20	9.99	1.20	2.35	0.70
35.1	13.42	1.43	9.48	1.43	3.94	0.86
40.1	14.55	1.36	10.02	1.36	4.54	0.91
45.1	15.54	1.43	9.72	1.43	5.82	1.04
55.1	16.73	1.49	9.50	1.49	7.23	1.18
65.1	18.15	1.62	8.52	1.62	9.62	1.41
75.1	18.52	1.63	8.17	1.63	10.34	1.41
85.1	18.92	1.22	7.85	1.22	11.07	1.53
95.1	18.73	1.68	6.93	1.68	11.80	1.54
115.1	18.54	1.71	6.90	1.71	11.63	1.51
135.1	16.88	1.88	5.62	1.88	11.25	1.53
155.1	15.45	1.58	4.34	1.58	11.11	1.44
195.1	12.94	1.27	3.16	1.27	10.07	1.31
245.1	11.69	1.27	2.54	1.27	9.16	1.27
295.1	11.05	1.46	2.52	1.46	8.53	1.13
395.1	10.07	1.27	2.11	1.27	7.95	1.07
495.1	7.93	1.33	1.56	1.33	7.07	0.90
595.1	7.53	1.33	1.21	1.33	6.02	0.79
795.1	7.13	0.87	1.27	0.87	4.86	0.66
995.1	5.80	0.93	1.20	0.93	4.60	0.63
1495.1	4.40	0.73	1.05	0.73	3.35	0.49
1995.1	3.73	0.53	1.13	0.53	2.61	0.39
2495.1	2.73	0.53	2.73	0.53		

knowledge, there are no other cross-section measurements or theoretical predictions to be compared with the present data.

The high-energy behavior of the electron-impact ionization cross section can be qualitatively described by the Bethe plot. For atoms or ions, the energy dependence of the ionization cross section σ_i can be satisfactorily represented by the following form:

$$\sigma_i = \frac{a}{E I_i}\left[\ln\left(\frac{E}{I_i}\right) + b\right]. \quad (8)$$

Here I_i (eV) represents the ionization threshold energy. The fitting parameters, a (cm^2 eV^2) and b, are determined by least-squares fit. The Bethe plot of the present ionization cross section data, on a logarithmic scale, shows that experimental data are adjusted along straight lines above 80 eV (Fig. 2). This indicates that the cross section is adequately described by the Born approximation. The core excitation may occur at higher electron energies but no break in linearity can be observed from the present Bethe plot, most likely because of the instability against predissociation of core-excited dications.

B. N^+ fragment production

This fragment originates from dissociative excitation (2) and dissociative ionization (4) reactions. The scans of the apparent cross section versus analyzer magnetic field are performed for electron energies of 11.1, 25.1, 95.1, and 295.1 eV. They are shown in Fig. 3. It has been demonstrated in a separate experiment [19], and confirmed in this experiment on simple ionization, that only fragments from the range $\Delta B/B = 0.007$ can be detected at a given magnetic field B. First, the transmission factors are determined as the ratio of the apparent cross section (integrated over ΔB) to the total signal integrated over the scan, for a given electron energy.

TABLE IV. Absolute cross sections (in 10^{-18} cm^2) for asymmetric dissociative ionization to C^{2+} (σ_{20}) and N^{2+} (σ_{02}) fragments.

E (eV)	σ_{20}	$\Delta\sigma_{20}$	σ_{02}	$\Delta\sigma_{02}$
33.1	0.15	0.20		
35.1	0.38	0.21		
40.1	1.13	0.26	0.00	0.13
45.1	2.05	0.39	0.24	0.16
50.1			0.55	0.17
55.1	2.93	0.47	0.97	0.26
65.1	3.42	0.54	1.15	0.27
75.1	3.64	0.59	1.29	0.27
80.1			1.68	0.32
85.1	3.81	0.61	1.88	0.33
90.1	4.09	0.63		
95.1	4.32	0.64	1.96	0.35
115.1	4.29	0.64	2.10	0.37
135.1	4.23	0.62	1.99	0.39
155.1	4.10	0.63	1.98	0.38
195.1	3.56	0.54	1.92	0.38
245.1	3.17	0.53	1.64	0.32
295.1	2.78	0.48	1.39	0.27
395.1	2.36	0.45	1.25	0.27
495.1	1.97	0.36	1.08	0.27
595.1	1.51	0.33	0.87	0.20
795.1	1.31	0.30	0.55	0.18
995.1	1.24	0.30	0.66	0.21
1195.1	1.00	0.23	0.49	0.16
1495.1	1.05	0.27	0.44	0.18
1995.1	0.57	0.20	0.42	0.20
2495.1	0.48	0.25	0.27	0.15

They range from 30% at 11.1 eV to 18% at 295.1 eV. By interpolation, correction factors are obtained for the whole electron energy range and the total absolute cross sections (σ_{N^+}) are determined. They are listed in Table II and also presented in Fig. 4, together with the estimated absolute error bars. Second, by use of the magnetic analyzer scans, presented in Fig. 3, fragment kinetic energy release distributions are

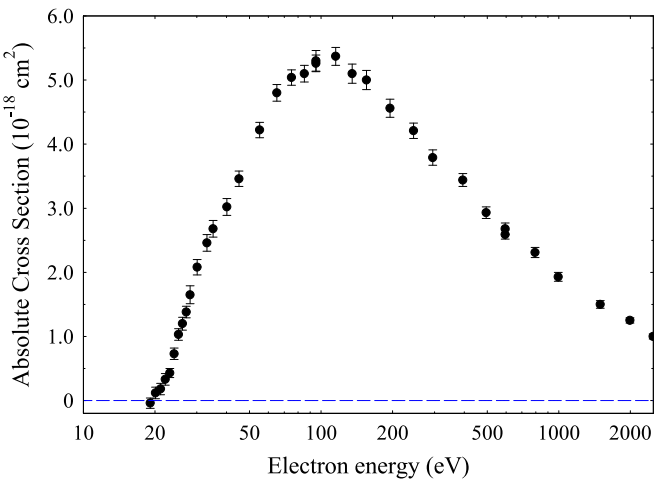

FIG. 1. Absolute cross sections for electron-impact simple ionization (σ_{SI}) of CN^+.

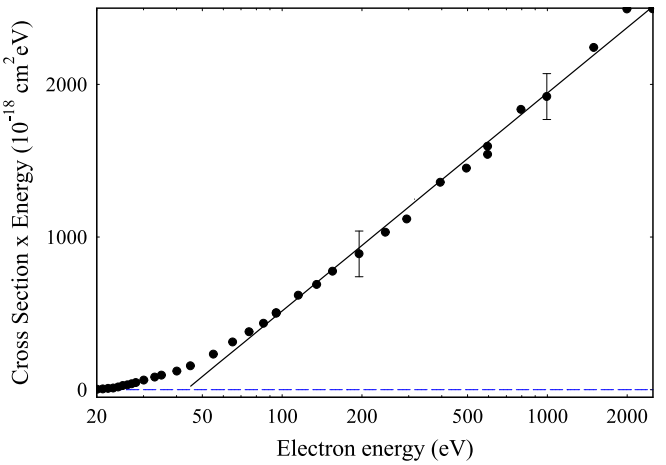

FIG. 2. Bethe plot for electron-impact simple ionization of CN^+.

determined for the selected electron energies. They are shown in Fig. 5.

As it can be seen from Fig. 5, the total energy liberated in the dissociation process extends to about 7 eV for lower electron energies and up to 14 eV for higher energies. The latter value is compatible with a vertical transition to a pure Coulomb potential-energy curve. Indeed, the equilibrium distance of CN^+ is 1.17 Å, which translates to 12.3 eV. These distributions, in general, exhibit two distinct contributions and are decomposed by fitting with multiple Gaussian functions. Based on the energy- and momentum-conservation arguments the two contributions are assigned to represent DE (low-energy peaks) and DI (high-energy peaks). The ratio of the DI and DE contributions (integrated over the corresponding peak areas) and the total absolute cross sections (σ_{N^+}) are further used to estimate absolute DI cross sections (σ_{11}) for the selected electron energies. By using the polynomial fit, DI cross sections are interpolated in the whole electron energy

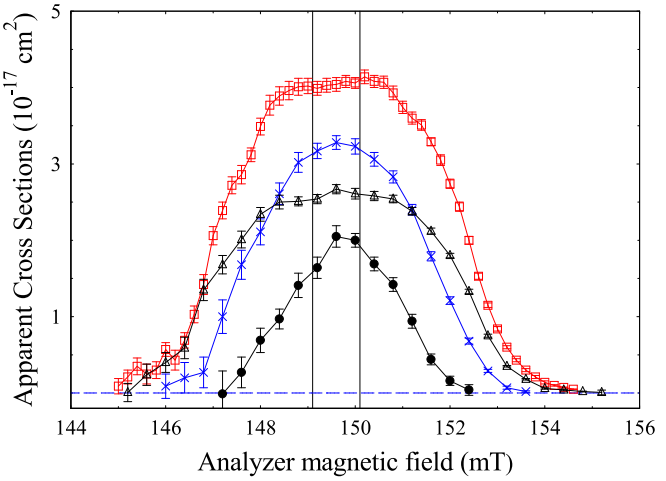

FIG. 3. Apparent cross sections for N^+ production as a function of the analyzer magnetic field. Electron energies are 11.1 eV (solid circles), 25.1 eV (crosses), 95.1 eV (squares), and 295.1 eV (triangles). The vertical lines indicate the acceptance window ΔB (see text). The lines connecting the marks are here to guide the eye.

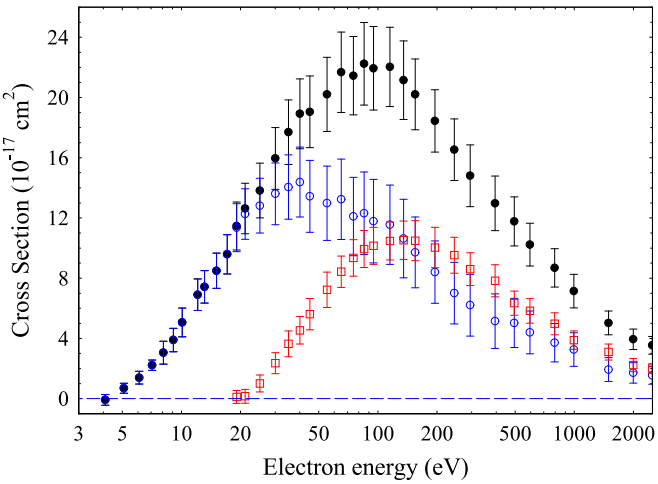

FIG. 4. Absolute cross sections for N^+ fragment production versus electron energy: total cross sections (σ_{N^+}, solid circles), dissociative excitation contribution (σ_{01}, open circles), and dissociative ionization (σ_{11}, squares).

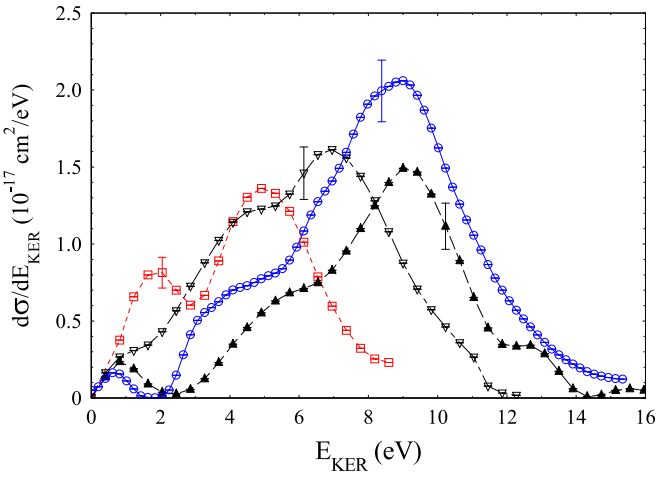

FIG. 5. Total KER distributions for N^+ fragment production. Electron energies are 11.1 eV (squares), 25.1 eV (open triangles), 95.1 eV (circles), and 295.1 eV (solid triangles).

range above the SI threshold. Finally, the DE cross sections (σ_{01}) are obtained by subtraction of the DI cross sections (σ_{11}) from the total absolute cross sections (σ_{N^+}). The total absolute cross sections for N^+ production and corresponding DE and DI cross sections are listed in Table II and are also shown in Fig. 4, together with the estimated absolute error bars. The total cross section for N^+ extends down to 4 eV. This value is compatible with the predicted dissociation energy of the CN^+ $^3\Pi$ state, 4.97 eV [16]. However, this first dissociation limit corresponds to $C^+ + N$, not $C + N^+$, which is expected to appear substantially higher in energy (8.28 eV from the $^1\Sigma^+$ vibrational ground state). Lower appearance energy implies the population of higher electronically excited states of the cation. The *ab initio* calculations by Hirst [15] predict six electronic states below the $C^+ + N(^4S)$ dissociation limit.

The total cross section exhibits a weak change of slope just above 8 eV and possibly another contribution at about 55 eV. It has a maximum of $(22.2 \pm 2.7) \times 10^{-17}$ cm^2 at 85 eV. The DE cross section follows the total cross section below the DI threshold. It has a maximum of $(14.4 \pm 2.3) \times 10^{-17}$ cm^2 at 40 eV and clearly shows the pronounced onset of a new contribution around 50 eV, which coincides with the inflection in the total cross section and is not related to the DI contribution.

In order to comprehend the complex structure exhibited by the DE cross section, the corresponding data presented in Fig. 4 have been fitted. Two types of contribution are possible, a resonant one defined in the introduction as RDE [26], and direct DE processes taken into account in Born-Bethe formalism appropriately modified to describe the cross-section behavior in the near-threshold region [21]. Three main contributions have thus been recognized from the present DE cross sections, the sum of which satisfactorily reproduces the experimental data.

A low experimental DE threshold can be attributed to RDE, i.e., to the initial capture of the incoming electron into a doubly excited state of CN, or into higher Rydberg series followed by autoionization to the vibrational continuum of the ground state [26]. Nevertheless, one cannot exclude the contribution of highly excited vibrational or metastable electronic levels of the target monocation. As already pointed out, metastable species are expected here, since the ions are created by ion-molecule reactions in the N_2 and CO mixture fed into the ion source.

The data from 4 to 7 eV are fitted and extrapolated to a wider energy region. This contribution is estimated to be about 2×10^{-17} cm^2 at 8 eV. After subtraction of this fit from the DE data, the next DE threshold is found to be 7.5 ± 0.5 eV. The slope of the cross section shows another contribution with onset at about 55 eV. Finally, at the high-energy side, the most likely inner shell contribution takes place above 400 eV. It would be uncertain to draw any definite conclusion about the importance of the various DE contributions in the low-energy region.

The threshold energy for the DI process is estimated to be at 20.6 ± 0.5 eV. The adiabatic DI threshold corresponding to the $C^+ + N^+$ ion pair is situated 19.5 eV above the CN^+ ground state, in perfect agreement with the present value and with Ref. [16]. This is similar to the SI result, 21.5 ± 0.5 eV. Thus it may be represented by the Bethe form of the cross section versus electron energy, expressed by Eq. (8), in the same way as σ_{SI}. Indeed, the Bethe plot of σ_{11} has a linear behavior above 100 eV. This fact at the same time confirms that the separation procedure was correct and that the extracted DI cross section represents the direct ionization process, as supposed.

As already described [19], based on the magnetic analyzer scans, fragment kinetic energy release distributions are determined for the selected electron energies. They are shown for the processes leading to N^+ fragment formation in Fig. 5. The total kinetic energy released to the fragments is presented for electron-impact energies of 11.1, 25.1, 95.1, and 295.1 eV. It ranges up to 14 eV, showing that more energetic fragments are produced at higher electron energies. Similar distributions are obtained for C^+ fragments and are discussed later. There are no other available data, to the authors' knowledge, to be compared with the present data.

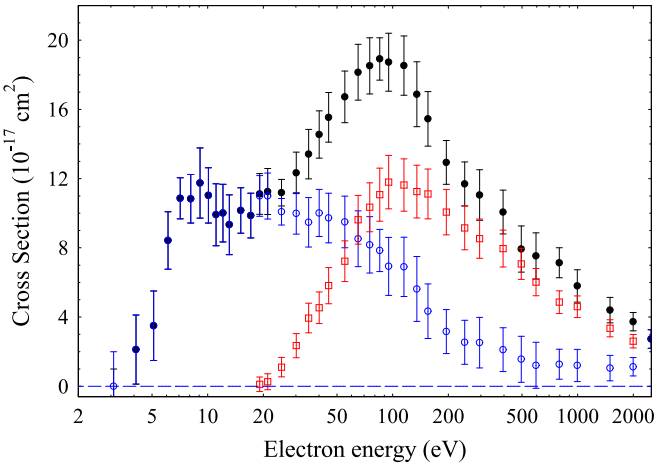

FIG. 6. Absolute cross sections for C^+ fragment production: total cross sections (σ_{C^+}, solid circles), dissociative excitation (σ_{10}, open circles), and dissociative ionization (σ_{11}, squares).

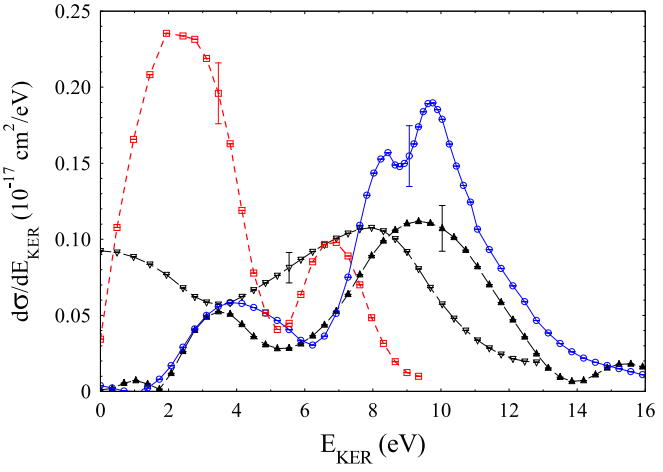

FIG. 7. Total KER distributions for C^+ fragment production. Electron energies are 11.1 eV (squares), 25.1 eV (triangles), 95.1 eV (circles), and 295.1 eV (solid triangles).

C. C^+ fragment production

The analyzer magnetic field scans for C^+ fragments have been recorded at select incident electron energies, identical to those used for N^+ fragments (11.1, 25.1, 95.1, and 295.1 eV). They have similar shapes and behavior as those for N^+ fragments, which are shown in Fig. 3. The widths of the C^+ fragment velocity distributions also increase significantly with the electron energy, in particular above the DI threshold, meaning that larger KER contributions are involved.

By our standard procedure and the data analysis method [19], as applied to N^+ fragments, these spectra are used to estimate absolute cross sections and kinetic-energy-release distributions for the dissociative processes leading to C^+ fragments. The total transmission factors are first determined as the ratio of the apparent cross section to the total signal integrated over the scan, for a given electron energy. They range from 32% at 11.1 eV to 16% at 295.1 eV. The transmission factors are obtained, by interpolation, over a wide electron energy range and are applied to determine the total absolute cross sections. The total cross sections for C^+ production are presented in Table III and also shown in Fig. 6, together with the corresponding absolute error bars. They represent the sum of the DE and DI cross sections.

By use of the magnetic field scans of the C^+ signal [19], kinetic-energy-release distributions are determined for the selected electron energies. These distributions are shown in Fig. 7. They clearly exhibit two distinct contributions. One, situated from 0 to 5.5 eV, is dominant at low electron energies. Another, more energetic, contribution is situated from 6 to 14 eV and is dominant at high incident electron energies.

Based on the energy- and momentum-conservation arguments the two contributions are assigned to represent the DE process (low-energy peaks) and the DI process (high-energy peaks). The ratio of the DI and DE contributions and the total absolute cross sections are further used to estimate absolute DI cross sections for the selected electron energies, as was done for N^+ fragments. By using a polynomial fit, DI cross sections are interpolated over the whole electron energy range above the SI threshold. Finally, DE cross sections are obtained by subtraction of the DI cross sections from the total absolute cross sections. Corresponding DE and DI cross sections for C^+ fragments are also presented in Fig. 6 and are listed in Table III, together with the estimated absolute error bars.

The threshold energy for dissociative ionization to C^+ should be the same as in the N^+ case, because DI arises in both cases from the same reaction (4) and the dynamics is thus the same for both fragments. The two fragments should have also the same DI cross-section values, if one neglects possible contribution via the double or multiple dissociative ionizations. Indeed, the absolute DI cross sections for C^+ fragments are in a reasonable agreement with those obtained for N^+ fragments. At about 115 eV, the maximums of the cross section for N^+ and for C^+ are observed to be essentially the same, within the estimated error bars. At 115 eV, DI cross sections are found to be $(10.5 \pm 1.3) \times 10^{-17}$ cm^2 and $(11.6 \pm 1.5) \times 10^{-17}$ cm^2 for N^+ and C^+, respectively.

The threshold energy for the DI process is estimated to be at 21.0 ± 0.5 eV. This is close to the value obtained from the N^+ signal, 20.6 ± 0.5 eV, and that for the SI process, 21.5 ± 0.5 eV. Thus, the two sets of DI data agree well with each other, confirming further the reliability of the separation procedure.

As in the N^+ case, below the DI threshold the total cross sections are equal to the DE cross sections σ_{10}, since only dissociative excitation contributes to the signal. The signal appears already from 3 eV and the maximum of σ_{10} is found to be $(11.7 \pm 2.0) \times 10^{-17}$ cm^2 at an electron energy of 9.1 eV. The threshold energy for the C^+ fragments is lower than for N^+ and in this low-energy region, up to 20 eV, σ_{10} is higher than σ_{01}. Above that energy, σ_{01} becomes significantly higher than σ_{10}. The threshold energies for the direct DE process, σ_{10}, are found at 6, 13, and 25 eV, respectively.

The maximum value of the total C^+ production cross section is found to be $(18.9 \pm 1.2) \times 10^{-17}$ cm^2 at an electron energy of 85 eV. A comparison can be made with the DE cross section for N^+ fragments, which is found to be $(22.2 \pm 2.7) \times 10^{-17}$ cm^2, also at 85 eV. Thus, at the maximum, the total cross section for C^+ production is some 15% lower than for the N^+ fragments.

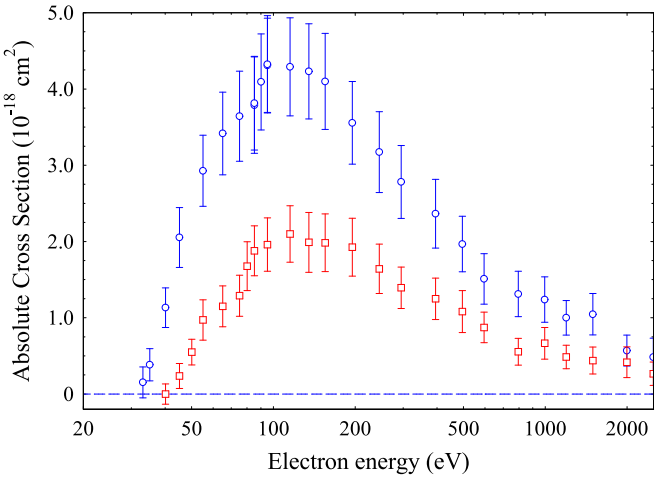

FIG. 8. Absolute cross sections for C^{2+} (σ_{20}, circles) and N^{2+} fragment (σ_{02}, squares) production versus electron energy.

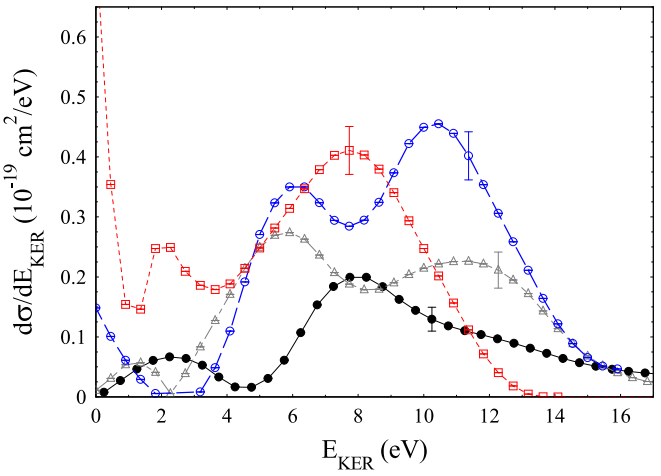

FIG. 9. Total KER distributions for C^{2+} fragment production at 55.1 eV (squares), 95.1 eV (open circles), and 295.1 eV (triangles) and for N^{2+} fragment production at 95.1 eV (solid circles).

A low C^+ experimental DE threshold can also be attributed in part to the presence of metastable levels of the target monocation. As already pointed out, the mixture of N_2 and CO used in the ion source may result in long-lived states ($^3\Pi$ and $^3\Sigma^+$) of CN^+, as already observed by Reid [17].

D. Asymmetric dissociative ionization, C^{2+} and N^{2+} fragment production

The asymmetric dissociative ionization has also been investigated, both for the C^{2+} and N^{2+} fragments, following reactions (5) and (6), respectively. Here, only the doubly charged particles are detected. Cross sections for any double-ionization process that would lead to the same fragments are considered to be negligible, as discussed by Siari *et al.* [31].

The analyzer magnetic field scans of the doubly charged atomic ions C^{2+} and N^{2+} are performed at select electron energies of 55.1, 95.1, 295.1, and 595.1 eV. These scans are used to normalize measured cross sections to the absolute scale and to determine KER distributions of the dissociation fragments, as stated in the introduction. First, for each scan, the transmission factor has been calculated. It ranges from 25% at low electron energy to about 10% for the higher energies. By using these results, the transmission factors are interpolated over the whole electron energy range, from the corresponding threshold up to 2.5 keV. In that way, absolute cross sections for ADI are determined, for both ions. The results are shown in Fig. 8 and also presented in Table IV, together with the corresponding error bars.

Absolute cross sections for C^{2+} are a factor of 2 higher than for N^{2+} over the whole electron energy range. The maxima of the cross sections are found to be $(4.3 \pm 0.6) \times 10^{-18}$ cm^2 at an electron energy of 95 eV for C^{2+} and $(2.1 \pm 0.4) \times 10^{-18}$ cm^2 at 115 eV for N^{2+}. The threshold energies are found to be 32.5 ± 1 eV for C^{2+} and 40.5 ± 1 eV for N^{2+}. The second ionization potentials of C and N are 24.4 and 29.6 eV, respectively. Combining these values with the dissociation energies of CN^+ to $C^+ + N$ and $C + N^+$, i.e., 4.97 and 8.28 eV, gives an adiabatic threshold of 29.4 and 37.9 eV for the production of C^{2+} and N^{2+}, respectively. These values are in reasonable agreement with the experimental findings.

The two sets of data have a similar behavior with energy. They both have pronounced change of the slope at about 75 eV, indicating possible contribution of a new process at this energy. At the high-energy side, both curves have an evident change of slope at about 800 eV. At this energy it may be due to contribution of an inner shell ionization channel. There are no other data, to the authors' knowledge, either for cross sections or for threshold energies, to be compared with the present results.

By using magnetic field scans of the detected signal, total KER distributions are determined for both fragments, at select electron energies. The results are shown in Fig. 9, for electron energies of 55.1, 95.1, and 295.1 eV for C^{2+} and for 95.1 eV for N^{2+}, respectively. In both cases, these distributions extend up to 16 eV and have dominant contributions between 5 and 12 eV, showing a number of individual peaks. At the present level of understanding, we cannot identify individual processes giving rise to these peaks.

E. Total dissociation and ionization cross sections

It is obvious from the above studied reactions that they lead to two main results: target particles may dissociate, or they may undergo simple or dissociative ionization, in both cases increasing the total number of particles or charges.

These processes are of particular interest for plasmas or gas discharges in environments containing the studied molecular ions. Knowing the cross sections for various reactions provides a reliable way to determine appropriate rate coefficients, which enable description of gas transport parameters and thus gas discharge evolution. In this section, present results are summarized in a manner to provide the total dissociation and ionization cross sections.

Reactions (2) and (3) represent dissociative excitation processes with the corresponding cross sections σ_{01} and σ_{10}. These are independent processes and the sum of the two cross sections is the total dissociative excitation cross section

which gives the probability for electrons to cause simple fragmentation of the CN^+ cation. The maximum of this cross section amounts to $(24.4 \pm 3.6) \times 10^{-17}$ cm^2 at an electron energy of 40 eV. The threshold for this signal coincides with the lower, C^+, onset at 3 eV and reaches a local plateau around 10 eV of about 1.6×10^{-16} cm^2.

As pointed out in the introduction, a detailed study of the total DE process has been published [18], based on storage ring measurements of the dissociative recombination and excitation of the CN^+ ion. Cross sections for the dissociative excitation represent the sum of σ_{01} and σ_{10}. In that experiment the neutral fragments C and N from reactions (2) and (3) were counted together, since they were not fully resolved by the detector. The threshold for total DE cross section was found to be 3.2 eV, which is in very good agreement with the present experiment. Based on the potential curves published by Hirst [15] for the vertical transition in the Franck-Condon region, the lower thresholds are associated to the dissociative limits $C^+(^2P) + N(^4S)$, $C^+(^2P) + N(^2D)$, and $C(^3P) + N^+(^3P)$ with energies of 5.0, 7.7, and 8.6 eV, respectively. The C^+ fragment has a lower threshold, but all listed energies are higher than experimental findings. In the actual experiment target cations were produced in the ground vibrational level ($v = 0$) of lowest-lying $^1\Sigma^+$ and $^3\Pi$ states by long-term storage, and their excitation in the ion source cannot explain the abnormally low threshold observed. A tentative explanation offered by Le Padellec *et al.* [18] is a "resonant enhanced" dissociative excitation process via autoionizing resonances. However, such an RDE process may only lead to bound CN^+ products below the first dissociation threshold. This explanation is further weakened by the fact that the DR high-energy peak is notably smaller than the DE peak in the energy range 3–5 eV, whereas DR and RDE share the same resonant electron-capture process.

Another striking feature displayed by the total DE cross sections in Ref. [18] is their exceptionally large magnitude at their plateau between 10 and 20 eV of approximately 8×10^{-16} cm^2. For N_2^+, O_2^+, CO^+, and NO^+ [18,24], values between 2×10^{-16} and 3×10^{-16} cm^2 have always been found, about three times smaller than those reported by Ref. [18]. The explanation for the huge CN^+ cross sections [18] would reside in the extremely high density of potential curves for CN^+, as calculated by Hirst [15], that may drive the DE process between 5.5 and 8 eV, i.e., just in the energy region where the DE signal rises up so sharply. However, present results do not support this hypothesis. In fact, our value of $(24.4 \pm 3.6) \times 10^{-17}$ cm^2 for the maximum of the total DE cross section of CN^+ fits just well in the range $(2–3) \times 10^{-16}$ cm^2, as measured for the other studied diatomics.

There are four reactions which contribute to the total ionization of CN^+. These are simple ionization (1), dissociative ionization (4), and two distinct ADI processes, (5) and (6). All corresponding cross sections are shown in Fig. 10. We believe that contributions from other possible ionization reactions, like double or multiple ionization, are negligible. They have much smaller cross sections and occur at higher electron energy [32].

The process of dissociative ionization (4) is identical for both fragments and follows simple ionization of the parent ion presented in reaction (1). Thus, the total electron-impact single ionization cross section of CN^+ represents the sum

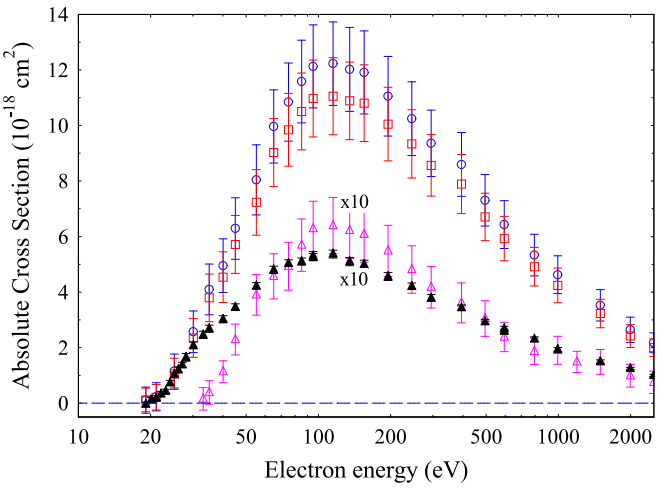

FIG. 10. Total ionization cross sections of CN^+ (open circles) and contributions of total ADI ($\sigma_{20} + \sigma_{02}$, open triangles), simple ionization (σ_{SI}, solid triangles), and DI (σ_{11}, squares).

of σ_{20}, σ_{02}, σ_{SI}, and σ_{11}. Here, the DI cross section is taken as a mean value of σ_{11} (C^+) and σ_{11} (N^+). The total ionization cross section is shown in Fig. 10, together with all contributing ionization cross sections, for comparison. The maximum of the total ionization cross section is found to be $(12.2 \pm 1.5) \times 10^{-17}$ cm^2 at an electron energy of 115 eV. We may consider individual contributions at the cross-section maximum to estimate the branching ratio of the ionization to different channels, since it remains nearly the same for all electron energies. The largest contribution is from DI, about 91%, then 5% from the asymmetric dissociative ionization and only 4% from SI. This proportion varies with electron energy, but at the same time depends on the energy of the primary ion beam. This dependence stems from the finite lifetime of the intermediate molecular dication states. All these states are metastable against dissociation and their fragmentation prior to detection varies with the ion flight time before they reach the detector.

The last statement can be demonstrated by the comparison of the above proportions with our recently published measurements of NO^+ ionization [24]. In that case, the dominant contribution comes from DI, about 65%, then 30% from SI and 5% from the asymmetric dissociative ionization. Thus, the ratio of SI to DI is 0.46 in NO^+ and only 0.04 in CN^+. It means that the fraction of doubly charged intermediate metastable ions which survive the time needed to reach the detector is much larger in NO^+. Having in mind the similar mass and energy of the two ions, i.e., nearly identical mean velocity, one can draw the conclusion that the mean lifetime of CN^{2+} is significantly shorter than that of NO^{2+}. We did not have the possibility to change the primary ion velocity enough to be able to determine those lifetimes.

A recent *ab initio* study of the CN^{2+} dication [30] predicts no less than 13 quasibound electronic states, 8 of which are not crossed by a purely repulsive curve. One would naively expect long-lived dications to be produced by electron-impact ionization of CN^+, in contradiction with our observations. The modest survival probability we deduce from the SI-to-DI

ratio may originate from the mismatch of the CN^+ and CN^{2+} equilibrium distance, as suggested by Ref. [30].

IV. SUMMARY AND CONCLUSIONS

Absolute cross sections for electron-impact ionization and dissociation of CN^+ ions leading to CN^{2+}, C^+, and N^+ as well as C^{2+} and N^{2+} ions were measured by applying the animated electron-ion crossed-beam method.

The maximum of the single ionization cross section was found to be $(5.37 \pm 0.14) \times 10^{-18}$ cm^2 at 115 eV. The measured threshold confirms the value obtained with synchrotron radiation [29].

The maximum total cross sections for C^+ and N^+ fragment production were observed to be $(18.9 \pm 1.2) \times 10^{-17}$ cm^2 and $(22.2 \pm 2.7) \times 10^{-17}$ cm^2 at 85 eV, respectively. Their thresholds lie significantly below the expected appearance energy, suggesting some contamination of the primary beam with electronically excited cations. More surprisingly, such a low threshold was also observed at the CRYRING storage ring [18], whereas no evidence for any high-lying initial electronic state could be gathered from the KER spectra measured for DR.

In order to have better control over initial electronic states, one should characterize their mixture resulting from the production of CN^+ in a CO/N_2 plasma, along the lines of the work performed by Reid [17]. The evolution of such a mix with long-term storage as performed by Le Padellec *et al.* [18] could also be modeled with the help of dedicated *ab initio* calculations.

The collected data were analyzed in detail in order to determine separately the DE and DI contributions to the total cross section for C^+ and N^+ fragment production. Present results for the total DE cross section are at the maximum about 2.4×10^{-16} cm^2 and are in significant disagreement with the cross sections of Le Padellec *et al.* [18], which are more than three times larger. However, the present value of the total DE cross section for CN^+ fits well among all other studied diatomics, regardless of the source of the data.

The DI and SI cross sections appear to be identical in shape close to their threshold, pointing to a common ionization process followed by Coulomb dissociation of the doubly charged radical. The SI-to-DI ratio is found to be much smaller than what was measured for NO^+ [24], reflecting the shorter predissociation lifetime of the CN^{2+} dication.

Cross sections for asymmetric dissociative ionization to C^{2+} and N^{2+} are more than one order of magnitude smaller. Their threshold is compatible with the sum of the CN^+ potential well depth and the appearance energy of the doubly charged products.

Kinetic-energy-release distributions of the fragment ions were analyzed and discussed for all considered fragments. The high-energy peak of the C^+ and N^+ distributions is compatible with pure Coulomb dissociation of the CN^{2+} dication into $C^+ + N^+$ pairs. This observation calls for a more detailed examination of the electronic states and vibrational levels likely to be populated by a vertical transition from CN^+ to CN^{2+}, and their survival probability on the time scale of the experiment, i.e., several microseconds.

ACKNOWLEDGMENTS

This work was supported by the Fonds de la Recherche Scientifique - FNRS through IISN Contract No. 4.4504.10. The authors value the financial support of the Association Euratom-Belgian State. D.S.B. is grateful for support from Project No. 171016 from the Ministry of Education, Science and Technological Development of the Republic of Serbia. The authors thank the Forschungszentrum Jülich for lending of the ECR ion source as well as all the staff members of the IMCN for their assistance in this experiment.

[1] J. B. Halpern, Y. Huang, and T. Titarchuk, Astrophys. Space Sci. **236**, 11 (1996).
[2] S. J. Bus, M. F. A'Hearn, D. G. Schleicher, and E. Bowell, Science **251**, 774 (1991).
[3] M. F. A'Hearn, R. C. Millis, D. O. Schleicher, D. J. Osip, and P. V. Birch, Icarus **118**, 223 (1995).
[4] N. Fray, Y. Bénilan, H. Cottin, M.-C. Gazeau, and J. Crovisier, Planet. Space Sci. **53**, 1243 (2005).
[5] A. Giannetti, J. Brand, F. Massi, A. Tieftrunk, and M. Beltrán, Astron. Astrophys. **538**, A41 (2012).
[6] S. Leach, Mon. Not. R. Astron. Soc. **421**, 1325 (2012).
[7] P. Thaddeus, Annu. Rev. Astron. Astrophys. **10**, 305 (1972).
[8] O. H. Crawford, A. C. Allison, and A. Dalgarno, Astron. & Astrophys. **2**, 451 (1969).
[9] A. C. Allison and A. Dalgarno, Astron. & Astrophys. **13**, 331 (1971).
[10] S. Harrison and J. Tennyson, J. Phys. B **45**, 035204 (2012).
[11] S. Harrison, J. Tennyson, and A. Faure, J. Phys. B **45**, 175202 (2012).
[12] J. Murrell, A. Al-Derzi, J. Tennyson, and M. Guest, Mol. Phys. **38**, 1755 (1979).
[13] P. J. Bruna, S. D. Peyerimhoff, and R. J. Buenker, Chem. Phys. Lett. **72**, 278 (1980).
[14] P. J. Bruna, S. D. Peyerimhoff, and R. J. Buenker, J. Chem. Phys. **72**, 5437 (1980).
[15] D. M. Hirst, Mol. Phys. **82**, 359 (1994).
[16] B. Jursic, J. Mol. Struct. THEOCHEM **498**, 123 (2000).
[17] C. Reid, J. Phys. B **27**, 4749 (1994).
[18] A. Le Padellec, J. Mitchell, A. Al-Khalili, H. Danared, A. Källberg, Å. Larson, S. Rosen, M. Af Ugglas, L. Vikor, and M. Larsson, J. Chem. Phys. **110**, 890 (1999).
[19] J. Lecointre, D. S. Belic, H. Cherkani-Hassani, J. Jureta, and P. Defrance, J. Phys. B **39**, 3275 (2006).
[20] J. Lecointre, S. Cherkani-Hassani, D. S. Belic, J. Jureta, K. Becker, H. Deutsch, T. Märk, M. Probst, R. Janev, and P. Defrance, J. Phys. B **40**, 2201 (2007).
[21] J. Lecointre, J. Jureta, and P. Defrance, J. Phys. B **43**, 105202 (2010).

[22] J. Lecointre, D. S. Belic, S. Cherkani-Hassani, and P. Defrance, Eur. Phys. J. D **63**, 441 (2011).
[23] D. S. Belic, J. Jureta, J. Lecointre, H. Cherkani-Hassani, S. Cherkani-Hassani, and P. Defrance, Eur. Phys. J. D **66**, 1 (2012).
[24] D. S. Belic, X. Urbain, H. Cherkani-Hassani, and P. Defrance, J. Phys. B **49**, 135202 (2016).
[25] I. Schneider, I. Rabadán, L. Carata, L. Andersen, A. Suzor-Weiner, and J. Tennyson, J. Phys. B **33**, 4849 (2000).
[26] C. Strömholm, J. Semaniak, S. Rosén, H. Danared, S. Datz, W. van der Zande, and M. Larsson, Phys. Rev. A **54**, 3086 (1996).
[27] P. Defrance, F. Brouillard, W. Claeys, and G. Van Wassenhove, J. Phys. B **14**, 103 (1981).
[28] P. Defrance, in *Atomic Processes in Electron-Ion and Ion-Ion Collisions* (Springer, New York, 1986), pp. 157–183.
[29] O. Kostko, J. Zhou, B. J. Sun, J. S. Lie, A. H. Chang, R. I. Kaiser, and M. Ahmed, Astrophys. J. **717**, 674 (2010).
[30] J. Fišer and R. Polák, Chem. Phys. **392**, 55 (2012).
[31] A. Siari, D. S. Belic, P. Defrance, and S. Rachafi, J. Phys. B **32**, 587 (1999).
[32] J. Lecointre, K. Kouzakov, D. S. Belic, P. Defrance, Y. V. Popov, and V. Shevelko, J. Phys. B **46**, 205201 (2013).